

Integration of Seismic and Well Log Data Using Acoustic Impedance for Lithology and Hydrocarbon Evaluation of “Ovi” Field, Niger Delta

Akpono Ejovi E^{a*}, Amigun John O.^b

^a*P.O. BOX 756, 25 Buba Maruwa Road, Satellite Town, Lagos. Nigeria*

^b*Department of Applied Geophysics, Federal University of Technology, P.M.B 704, Akure. Nigeria*

^a*Email: akponoejovi@gmail.com*

^b*Email: johnamigun@gmail.com*

Abstract

This research work is aimed at using acoustic impedance as means of predicting lithology and hydrocarbon away from well control of “Ovi” Field hence providing a detailed evaluation of the hydrocarbon potential of the area. The methodology used involves identification of hydrocarbon bearing reservoirs from well logs using Gamma ray and resistivity logs, wells correlation, petrophysical analysis, well to seismic tie, horizon and fault mapping, generation of structural maps, acoustic impedance crossplot analysis and seismic inversion using model based approach. Three reservoir sand were mapped within the Agbada Formation. From the crossplot of acoustic impedance against gamma ray, porosity and water saturation, the acoustic impedance ranges from 24500-27500 (ft/s)*(g/cc) for shale and 17500-24500 (ft/s)*(g/cc) for sand based on the saturating fluids, the results also shows that acoustic impedance have a linear relationship with water saturation, while porosity have an inverse relationship with acoustic impedance for the study area. Average acoustic impedance maps for reservoir tops generated from the inverted seismic data indicated areas of low acoustic impedance corresponding to hydrocarbon bearing zones that were not detected on the time maps. The result provided detailed information about the subsurface lithology and hydrocarbon saturation away from well control of the study area.

Keyword: Hydrocarbon; Acoustic Impedance; Inversion; Crossplotting.

* Corresponding author.

1. Introduction

One of the critical challenges in hydrocarbon exploration is the assessment of reservoir quality beyond areas covered by wells. One technique that attempts to provide the prediction of reservoir properties from seismic data and solve this problem is seismic inversion. Integration of seismic and well log data can aid the proper understanding of reservoir characterization in order to optimize hydrocarbon production. However, by estimating acoustic impedance from logs and establishing a relationship among various reservoir properties through the analysis of 3D seismic inversion we can determine reservoir properties beyond well locations [10]. Seismic inversion is a process that converts seismic trace information into acoustic impedance. Through the inverted impedance other reservoir properties such as lithology, porosity and fluid content can be quantified away from the well. The inverted impedance model can also be used for building facies and facies based porosity and permeability model [9].

Seismic inversion involves converting the reflectivity seismic data into acoustic impedance by using suitable wavelets. Different seismic inversion methods (such as Model Based, Band limited, Sparse Spike and Stochastic) are used commercially to map the detailed reservoir properties such as lithology and fluid properties. These properties are estimated by using different inversion algorithms on the seismic data with prior geological knowledge and well log data. The relationship between seismic and lithology is empirical. The reduction of uncertainty in this relationship will have large effect on the reservoir model building, thus on development and production of the hydrocarbon [2]. The inverted impedance model is also used for building facies and facies based porosity and permeability model [9].

Correlation between seismic average impedance and log-derived impedance can aid better understanding of formation lithologies and cross plots of acoustic impedance can also be used to study the lithology of a given formation and the saturating fluid [1]. Discrimination of sand from shale, detection of stratigraphic trap such as pinch outs and encasement of sand within shale are easier to detect in impedance section than in stacked seismic sections, it therefore better to scan through volume of inverted seismic data to map favorable hydrocarbon sand reservoir. Acoustic impedance can be used as an indicator of lithology, porosity and even the presence of hydrocarbon, it can also be used as a qualitative and quantitative reservoir analysis and mapping of flow units [10].

In this study post-stacked seismic inversion was carried out using model based approach by integrating seismic and well log data to characterize and predict the reservoir parameters of "Ovi" Field based on acoustic impedance.

1.1 location and geology

"Ovi" Field is situated within the onshore Niger Delta, located in southern Nigeria between Longitudes 3-9°E and Latitudes 4-6°N. Figure 1 shows the study location.

The Niger Delta is situated in the Gulf of Guinea and extends throughout the Niger Delta Province. From the

Eocene to the present, the delta has prograded southwestward, forming depobelts that represent the most active portion of the delta at each stage of its development [3]. The continental basement exhibits two structural elements [7]. The onshore portion of the Niger Delta province is delineated by the geology of southern Nigeria and southwestern Cameroon (figure 1).

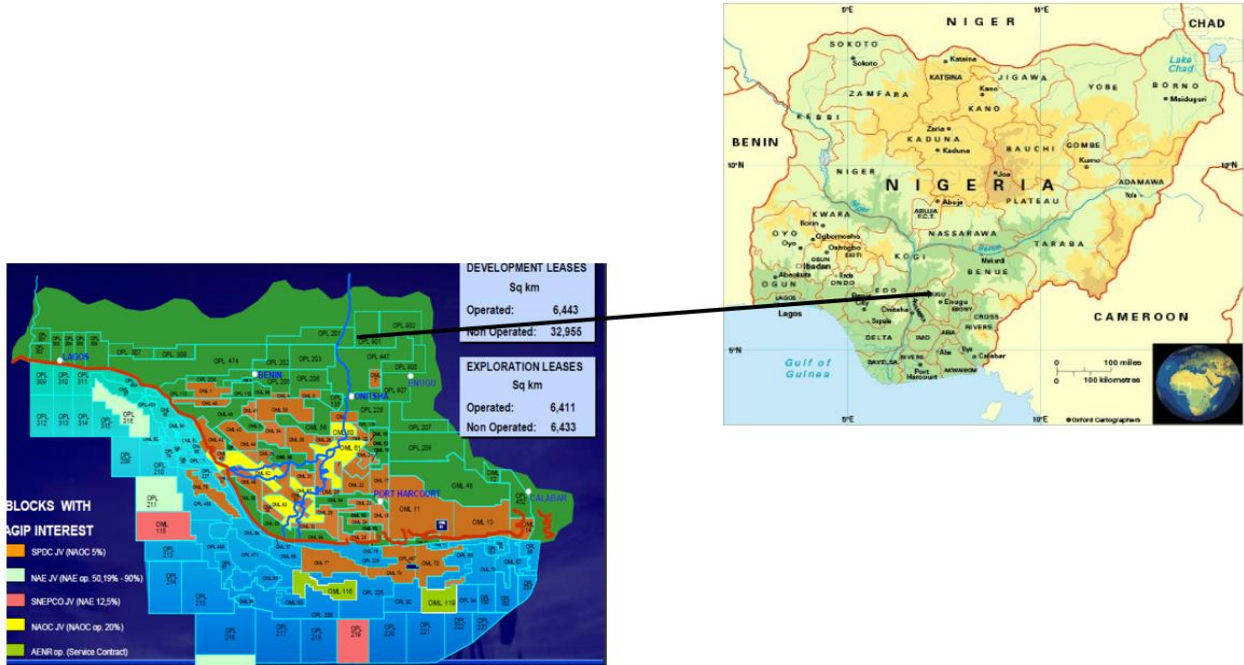


Figure 1: Geologic Map of Niger Delta

The northern boundary is the Benin flank, an east-northeast trending hinge line south of the West Africa basement massif. The northeastern boundary is defined by outcrops of the cretaceous on the Abakaliki High and further east-southeast by Calabar flank a hinge line bordering the adjacent Precambrian. The offshore boundary of the province is defined by the Cameroon volcanic lines to the east, eastern boundary of the Dahomey basin (the eastern-most West Africa transform-fault passive margin) to west, and the two kilometer sediment thickness contour or the 4000-meter bathymetric contour in areas where sediment thickness is greater than two kilometers to the south and southwest.

The province covers 300,000km² and includes the geologic extent of the Tertiary Niger Delta (Akata-Agbada) Petroleum System [6].

According to the authors in [9] the Niger Delta consist of three formations: the continental top facies (Benin Formation), the Agbada Formation and the Akata Formation.

The Benin formation is the shallowest of the sequence and consists predominantly of fresh water-bearing continental sands and gravels. The Agbada Formation underlies the Benin Formation and consists primarily of sand and shale and is of fluviomarine origin. It is the main hydrocarbon-bearing window. The Akata Formation is composed of shales, clays and silts at the base of the known delta sequence. They contain a few streaks of

sand, possibly of turbiditic origin. The thickness of this sequence is not known for certain, but may reach 7000m in the central part of the delta [8]. Petroleum in the Niger Delta is produced from sandstone and unconsolidated sands predominantly in the Agbada Formation. The characteristics of the reservoirs in the Agbada Formation are controlled by depositional environment and the depth of burial. Known reservoir rocks are Eocene to Pliocene in age and are often stacked, ranging in thickness from less than 15 meters with about 10% having greater than 45 meters thickness [4]. The thicker reservoirs represent composite bodies of stacked channels [3].

Niger delta fields are dominated by mostly structural traps and stratigraphic traps. The structural traps developed during syn-sedimentary deformation of the Agbada paralic sequence [4,11]. Structural complexity increases from the north (earlier formed depobelts) to the south in response to increasing instability of the under-compacted, over-pressured shale. The authors in [3] described a variety of structural trapping elements, including those associated with simple rollover structures clay-filled channels, structures with multiple growth faults, structures with antithetic faults and collapsed crest structures. On the flanks of the delta, stratigraphic traps are likely as important as structural traps. In this region, pockets of sandstone occur between diapiric structures. Towards the delta toe (base of distal slope) this alternating sandstone-shale sequence gradually grades to essentially sandstone.

1.2 Materials and methods

The materials used for this study includes a 3-D seismic data and suite of wireline data which consist of sonic, density, gamma ray, resistivity and porosity logs. The work flow adopted for this work is shown in figure 2. Acoustic impedance provides better understanding of reservoir due to its relationship with various petrophysical parameters such as porosity, lithology and fluid content. Prior to the seismic inversion, Crossplot analysis was carried out in the well domain to establish the relationship between acoustic impedance and porosity (ϕ), water saturation (S_w) and gamma ray reading. Model based inversion was carried out by integrating seismic and well log data using the strata module of the Hampson Russell software package. Quality control of the data was done to check for washouts and other bad borehole conditions that can affect the log reading and lead to wrong interpretation. The synthetic trace was generated from the well logs and the Checkshot data was used to convert depth to two way travel time. In other to generate the synthetic trace density and Primary wave (p-wave)log values were combined to get reflectivity spikes, this procedure was done repeatedly for four wells (well2, well3, well4, and well12). A wavelet was first extracted from the real seismic data which is known as statistical wavelet. This statistical wavelet is symmetrical in shape as shown in Figure 3a. The second wavelet was extracted from the well log data and is called wavelet using wells. This wavelet is non symmetrical and is generated from well logs as shown in Figure 3b. These wavelets were then convolved with the reflectivity spike one after the other in order to get a synthetic trace. The synthetic trace obtained was correlated with the average seismic trace around the well bore. Synthetic trace using statistical wavelet was first correlated and is shown in Figure 4a. From Figure 4a, it is clear that the synthetic does not match well with the real seismic data and the correlation coefficient value is small. The software Hampson Russell manual suggested shifting down of the synthetic trace to improve the correlation coefficient as shown in Figure 5a. The synthetic trace using wavelet from wells was also correlated with average seismic data. The software suggested 1ms downward shift of synthetic trace shown in Figure 5b. After applying this shift of synthetic trace the synthetic and the real seismic

matched well as shown in Figure 4b. The suggested shifting depends on the correlation window chosen. It is very safe to have small time window to have a good match. The low frequency initial model was generated in order to guide inversion. It involves the multiplication of density and sonic from each of the wells to produce acoustic impedance logs. There after the converted acoustic impedance logs were filtered with 10Hz high cut filter to generate an initial model. The filtered logs are interpolated between and beyond the holes guided by the imported horizon from 2200ms-3200ms which is the area of interest. Three initial models were recursively iterated with processing sampling rate of 2ms to predict the best acoustic impedance log and synthetic seismic data. The well-matched logs are also interpolated throughout the input seismic profile guided by control horizons (Russell and Hampson 1991). From the quality control Panel (Figure 6) there is reasonably good agreement between the inverted (red line) and computed acoustic (blue line) impedance within a constraint window. The black curves indicate the low-frequency impedance extracted from the observed impedance logs. The comparison of the real seismic data and that predicted by the acoustic impedance logs and the estimated source wavelet at the well shows a near perfect match with a good correlation coefficient for well 12, 2, 3 and 4 which shows that the Inversion result gave a good quality acoustic impedance value for the inter-well regions. There after the seismic data was inverted.

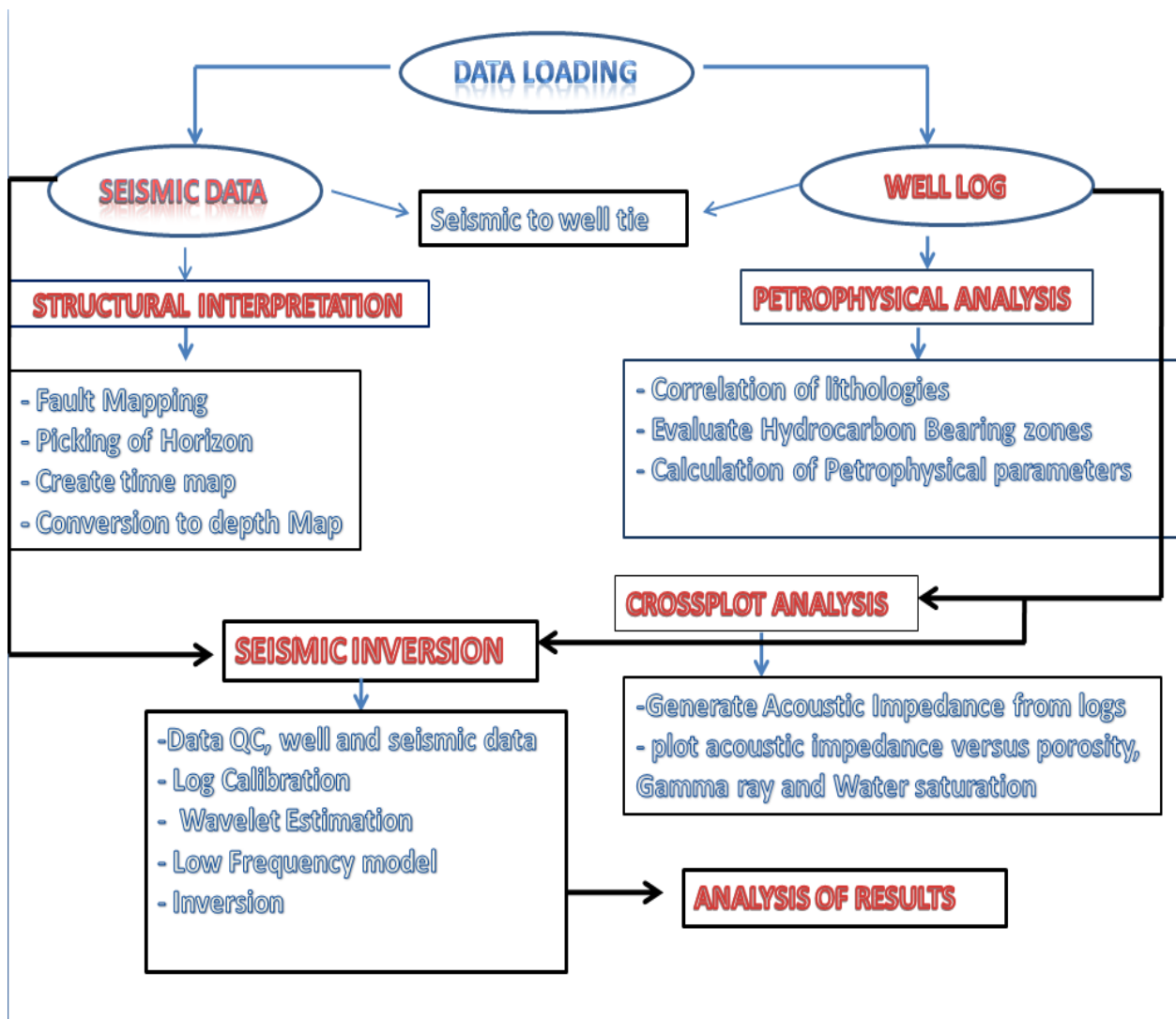


Figure 2: Flow Chart of Methodology

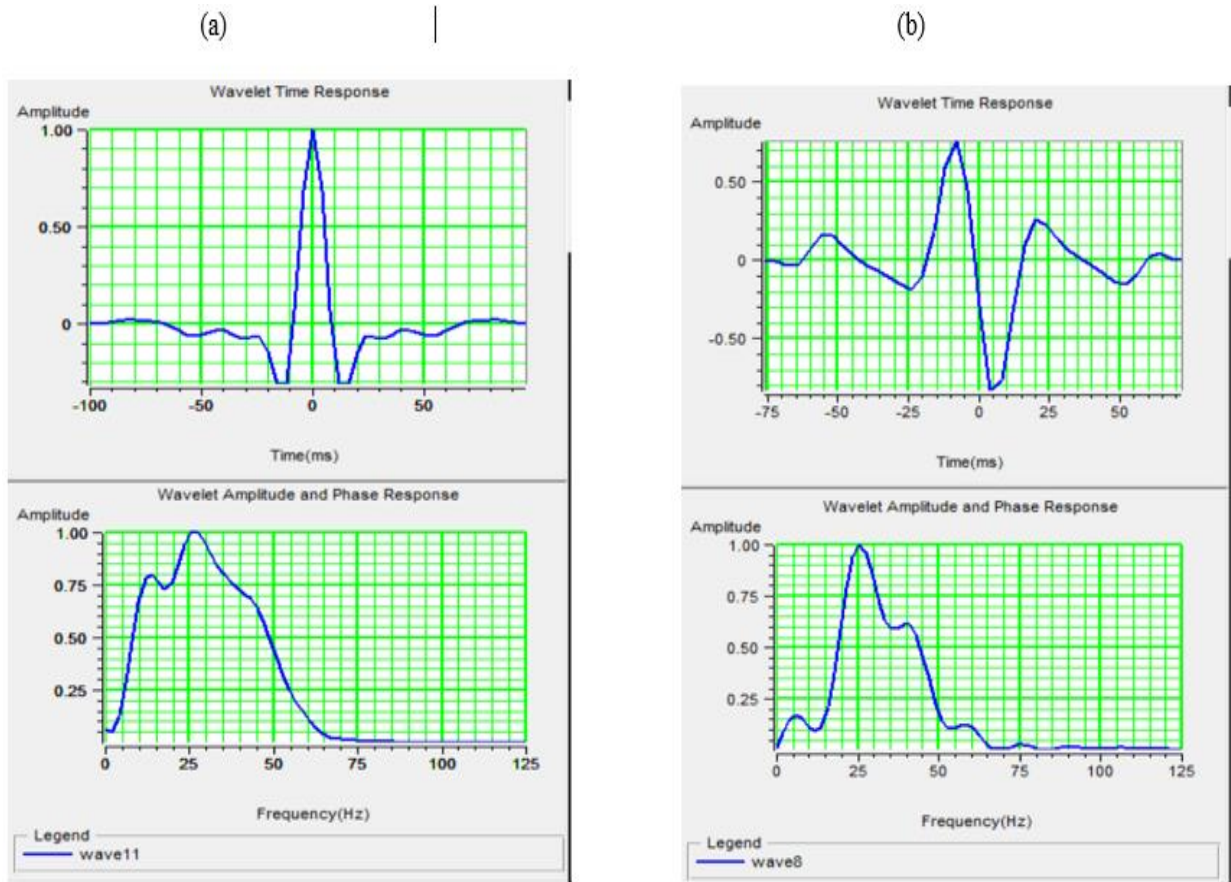
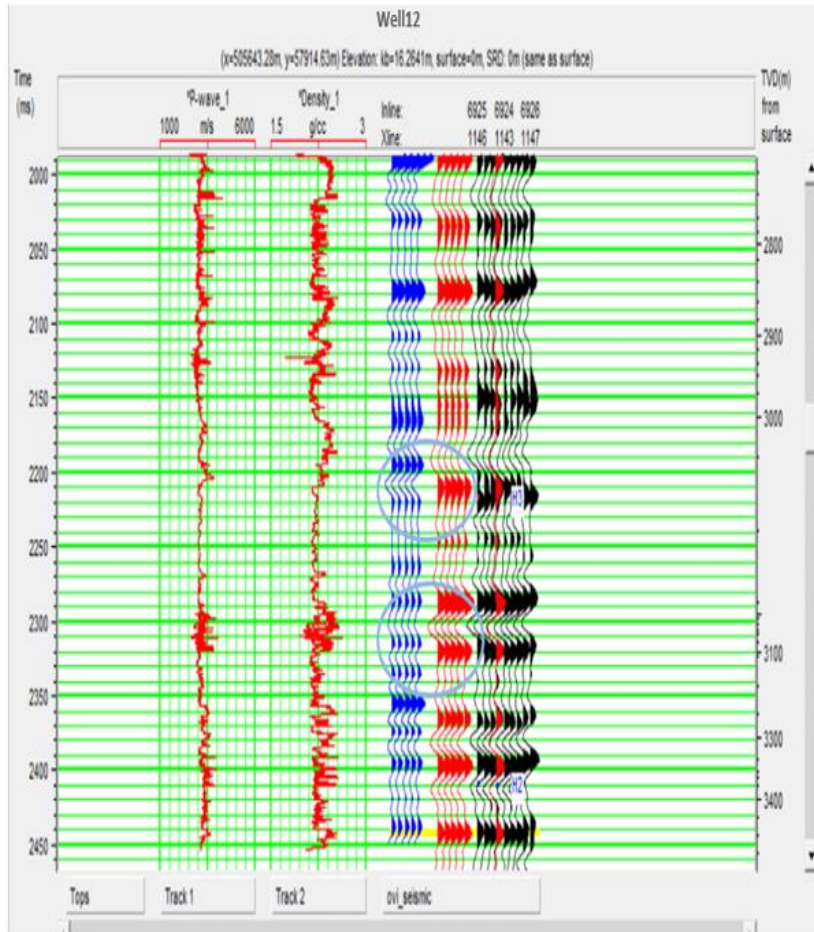


Figure 3: Wavelets Extracted. (a) Statistical (b) Using well

(a)



(b)

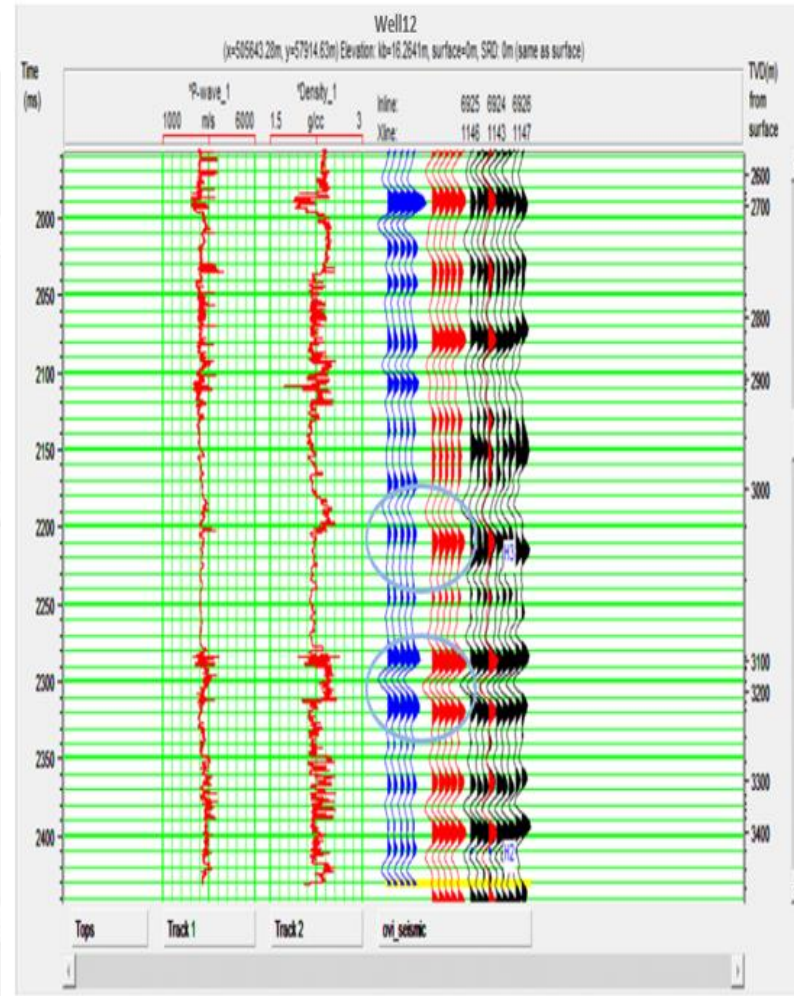


Figure 4: Synthetic Trace Generated (blue) (a) Using Statistical Wavelet (b) Using Well Wavelet

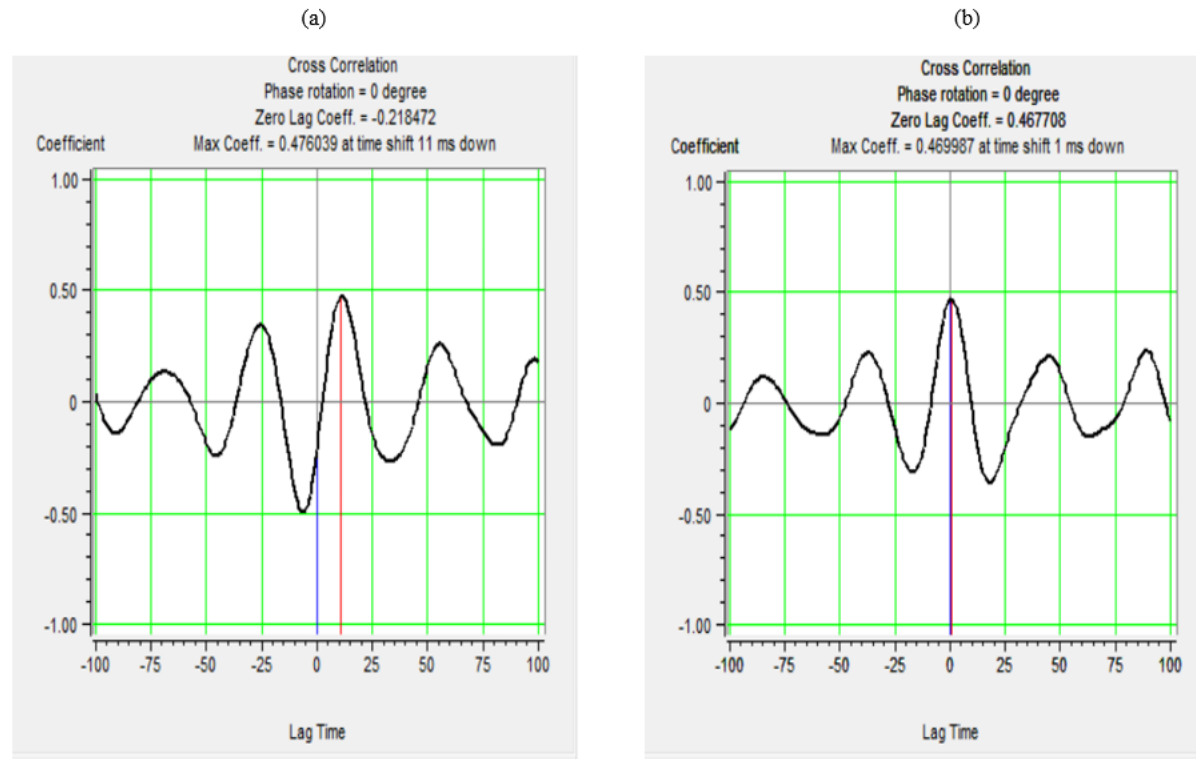


Figure 5: Time Lag of the Synthetic Trace Represented by Blue Line, Overlying with Minute

Difference of Red Line of Composite Trace. (a) Generated from Seismic Data (b)

Generated from Well log

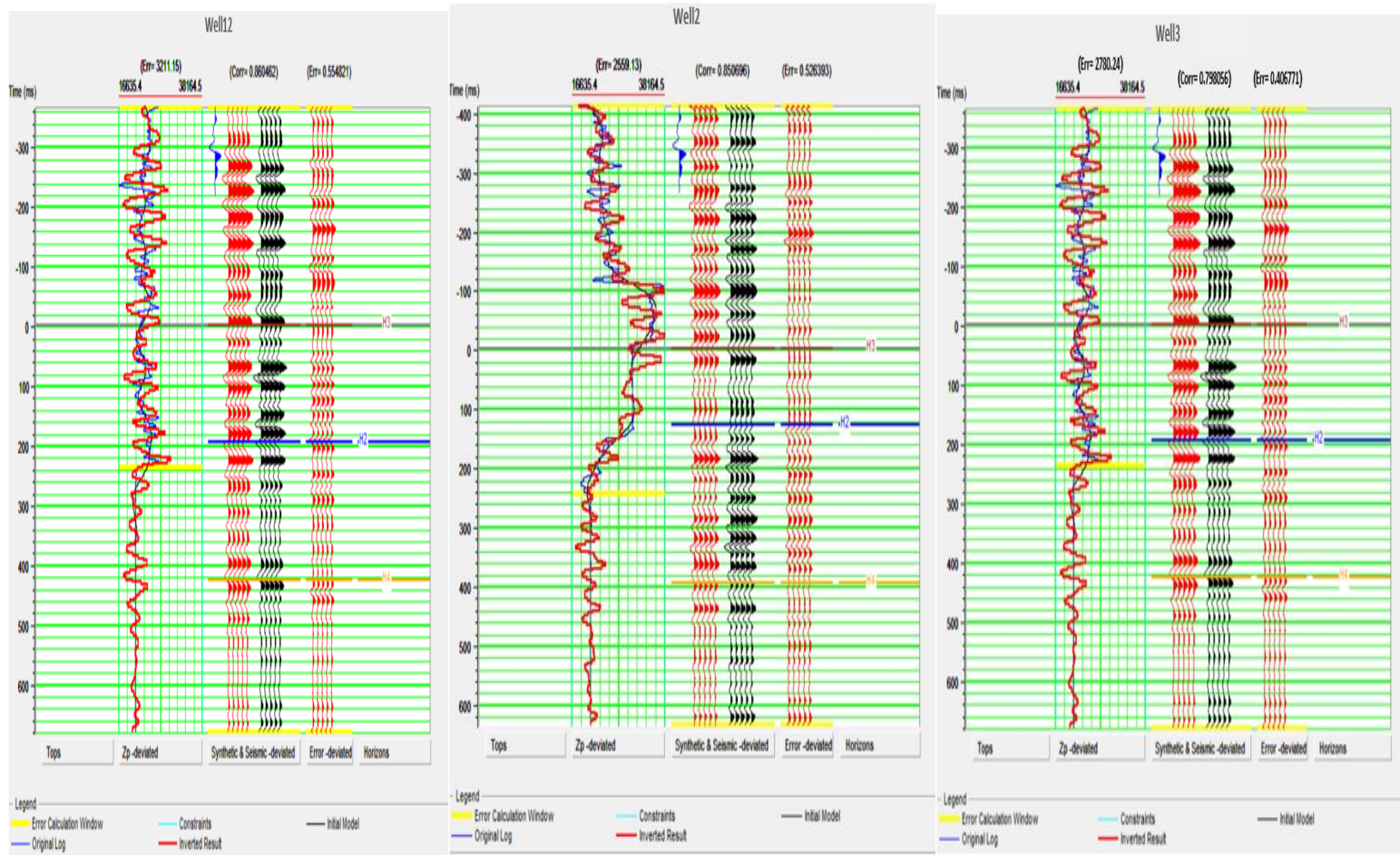


Figure 6: Quality Control for Panel for seismic inversion at the well bore (a) well3 (b) well4 and (c) well3 showing the inverted (red line) and computed acoustic (blue line) impedance within a Constraint window.

1.3 Discussion and results

Three sands were picked across the wells which are named Sand A (reservoir A), sand B (reservoir B), and sand C (reservoir C), the sands are capped by shale (Figure 7). The average computed petrophysical parameters are shown in Table 1 with gross thickness ranging from 32.62 to 59.13m, net thickness ranging from 24.53 to 34.70m, Net/Gross ranging from 0.56 to 0.75, porosity values ranging from 31 to 34%, effective porosity ranging from 20 to 22%, permeability ranging from 2879 to 3500mD and the hydrocarbon saturation ranging from 60 to 61%. This results show that the reservoirs of interest have high hydrocarbon saturation, good porosity and they are viable.

The crossplot of acoustic impedance and gamma ray values (Figure 8a) shows three lithologies which were inferred based on the cluster and where they fall under the gamma ray axis using a cut off of below 65API as sand and above 65API as shale. Clusters that are associated with shale falls in the impedance range of 24500 to 27500(ft/s)*(g/cc), while those associated with water bearing sands falls in the impedance range of 22000 to 24500(ft/s)*(g/cc) and clusters associated with hydrocarbon bearing sand falls in the impedance range of 17500 to 21500(ft/s)*(g/cc).

Figure 8b confirms this as it shows an abrupt decrease of Acoustic impedance log reading for reservoir A having hydrocarbon compare to that of shale and water bearing sand, this validates the cross plot analysis.

Figure 9 shows the cross plot of porosity and acoustic impedance for well 2 and well 12. From the crossplot porosity shows an inverse relationship with acoustic impedance and this was confirmed in most of the wells. This crossplot shows that the porosity reduces as the acoustic impedance increases and vice versa. Areas of low acoustic impedance are associated with high porosity. Figure 10 shows the crossplot of water saturation and acoustic impedance. Acoustic impedance shows a linear relationship with water saturation. Water saturation increases with acoustic impedance and this relationship is also obtained in most of the wells.

The acoustic impedance values observed at inline 6925 were categorized and color coded in six zones as shown in table 2. The inverted seismic section on inline 6925 (Figure 11) shows that the three horizons falls on impedance range associated with sand from the crossplot analysis 17500-24500(ft/s)*(g/cc). Average acoustic impedance map were generated with a time window of 5ms covering the three horizons of interest, these impedance maps shows area with lower acoustic impedance with wells penetrated. The position of the wells on the impedance map validates the results of the inversion. Figure 12, 13 and 14 show the average acoustic impedance map for horizon H1, H2 and H3 respectively. All hydrocarbon bearing zone are characterized by low acoustic impedance as established from the crossplot analysis. From the maps zones of low impedance are also characterized by high porosity and low water saturation as established from the crossplot analysis. Table 3, 4 and 5 summarize the acoustic impedance values for horizon H1, H2 and H3 respectively. The Table shows wells that penetrated each zone on the acoustic impedance map, porosity values of the wells and the prospect areas mapped. Prospect areas mapped are based on low acoustic impedance that falls within the range of values for hydrocarbon bearing sand from the crossplot analysis.

Three prospect X, Y and Z were identified on horizon H1 impedance map while two prospect A and B were identified on horizon H2 impedance map and two prospects P and Q were identified on horizon H3 impedance map.

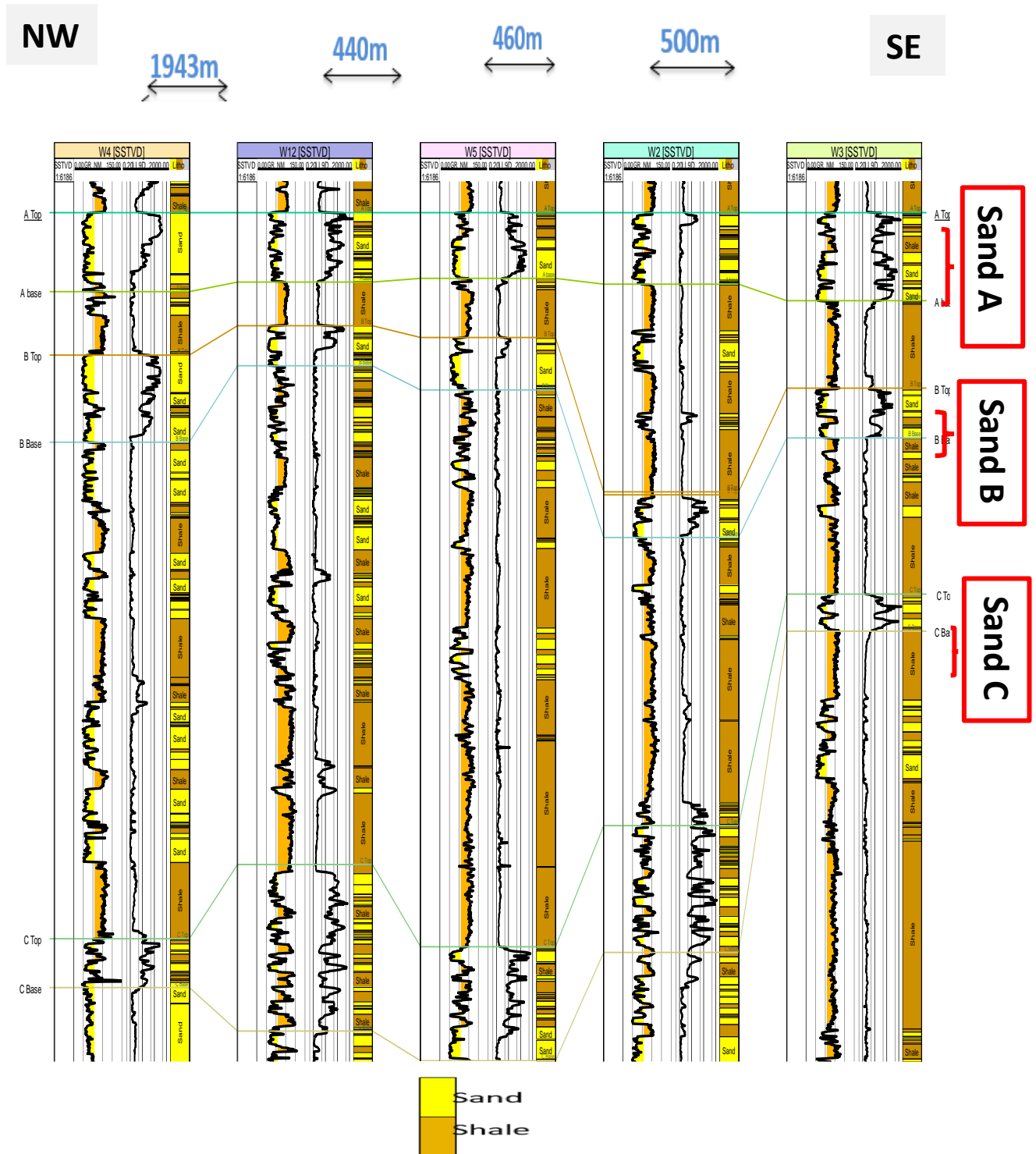


Figure 7: Well Correlation Panel showing Well 4, 12, 5, 2, 3. It describes the Reservoirs

Correlation across the five Wells.

Table 1: Average Computed Petrophysical Parameters for the Three Reservoir of Interest

Name	Gross thickness (m)	Net pay (m)	Net/gross	Porosity (frac)	Sw (%)	Permeability (mD)	Sh(%)	Vsh(%)	Φ_{eff}
Sand A	44.50	34.70	0.75	0.34	0.40	2960	0.61	0.11	0.22
Sand B	32.62	24.53	0.72	0.31	0.38	3294	0.60	0.10	0.20
Sand C	59.13	32.14	0.56	0.31	0.40	2879	0.61	0.12	0.21

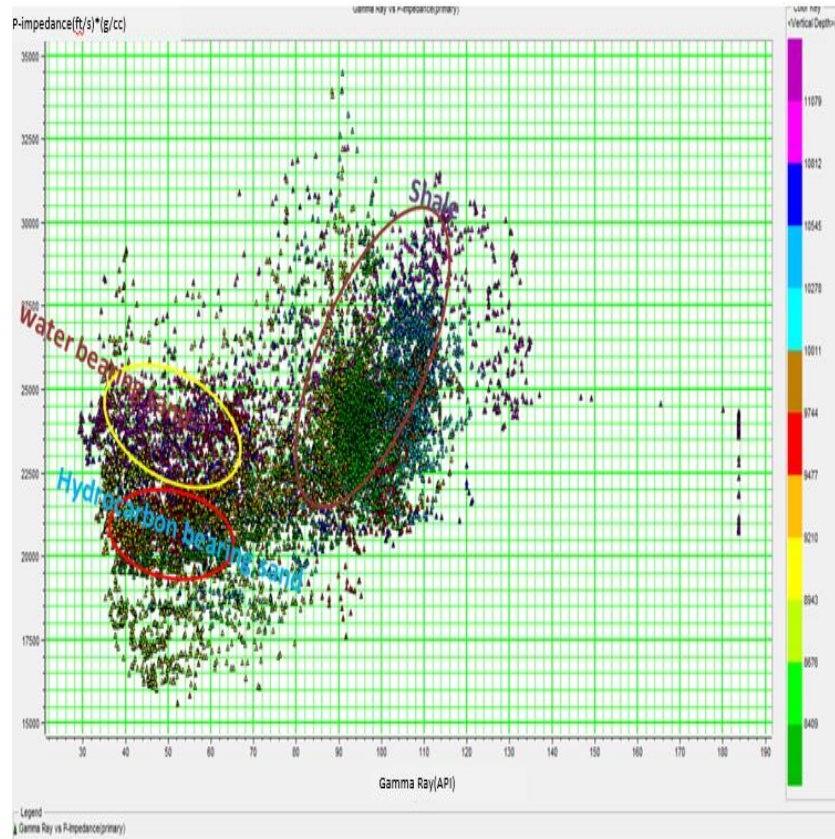


Figure 8a: Cross Plot of Acoustic Impedance and Gamma

Ray Reading for Well 12

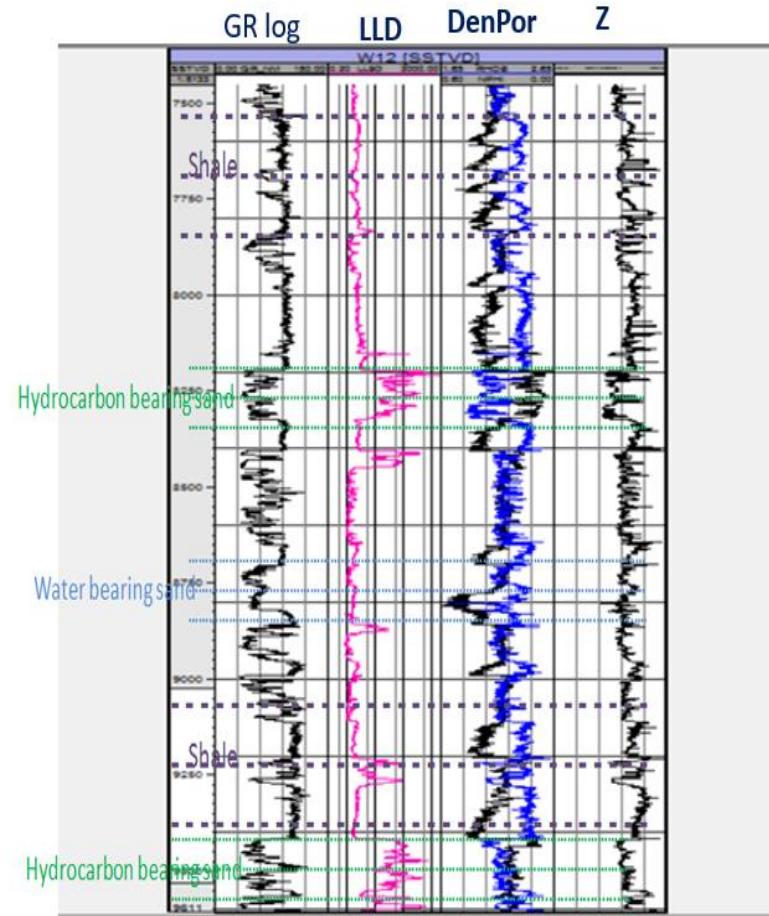


Figure 8b: Correlation Panel of Well 12 Showing an Abrupt

Decrease in Impedance in area Suspected to be Hydrocarbon

(a)

(b)

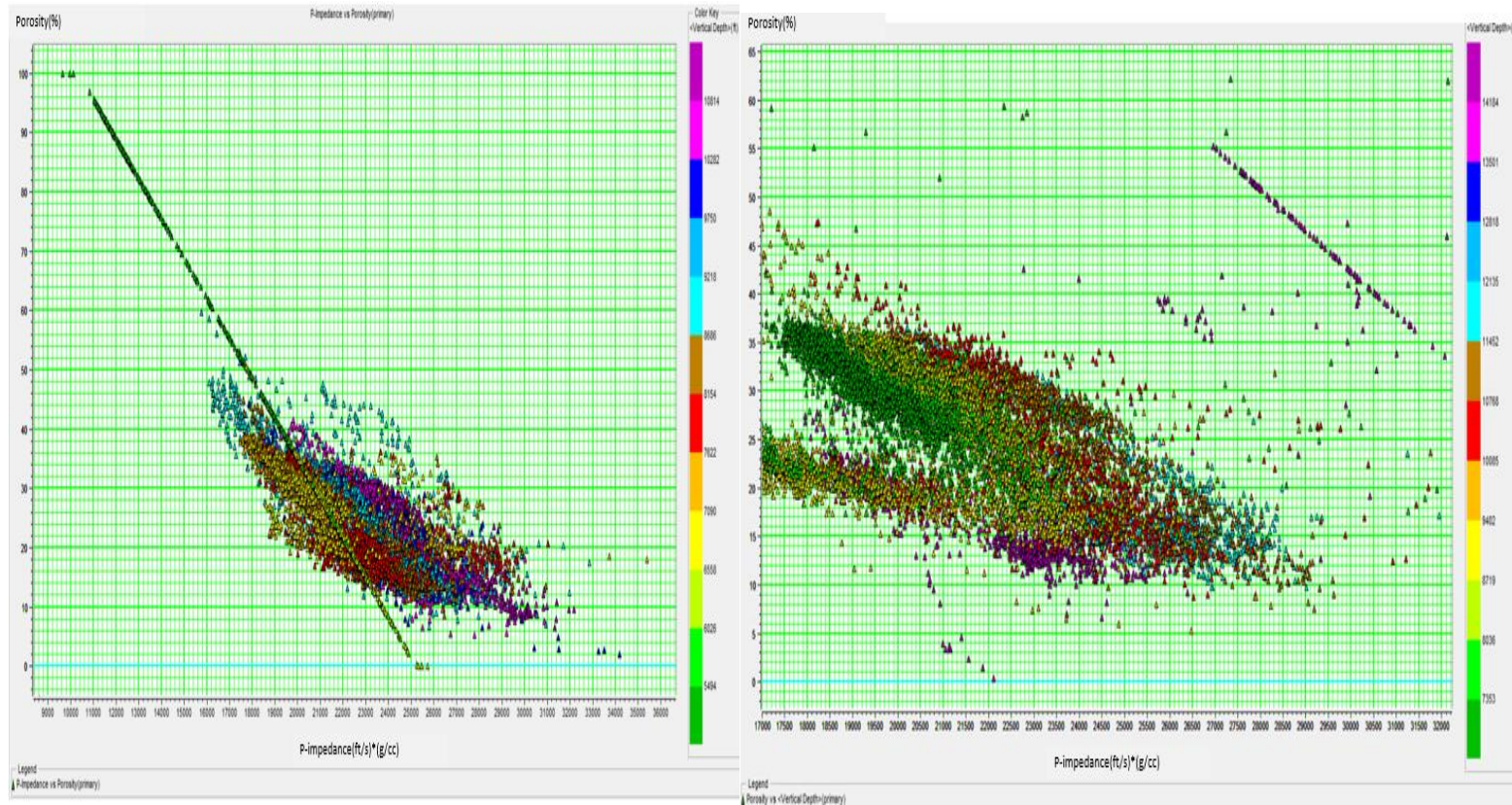


Figure 9: Crossplot of Porosity versus Acoustic Impedance for (a) Well 2 (b) Well12 Showing a Linear Relationship

(a)

(b)

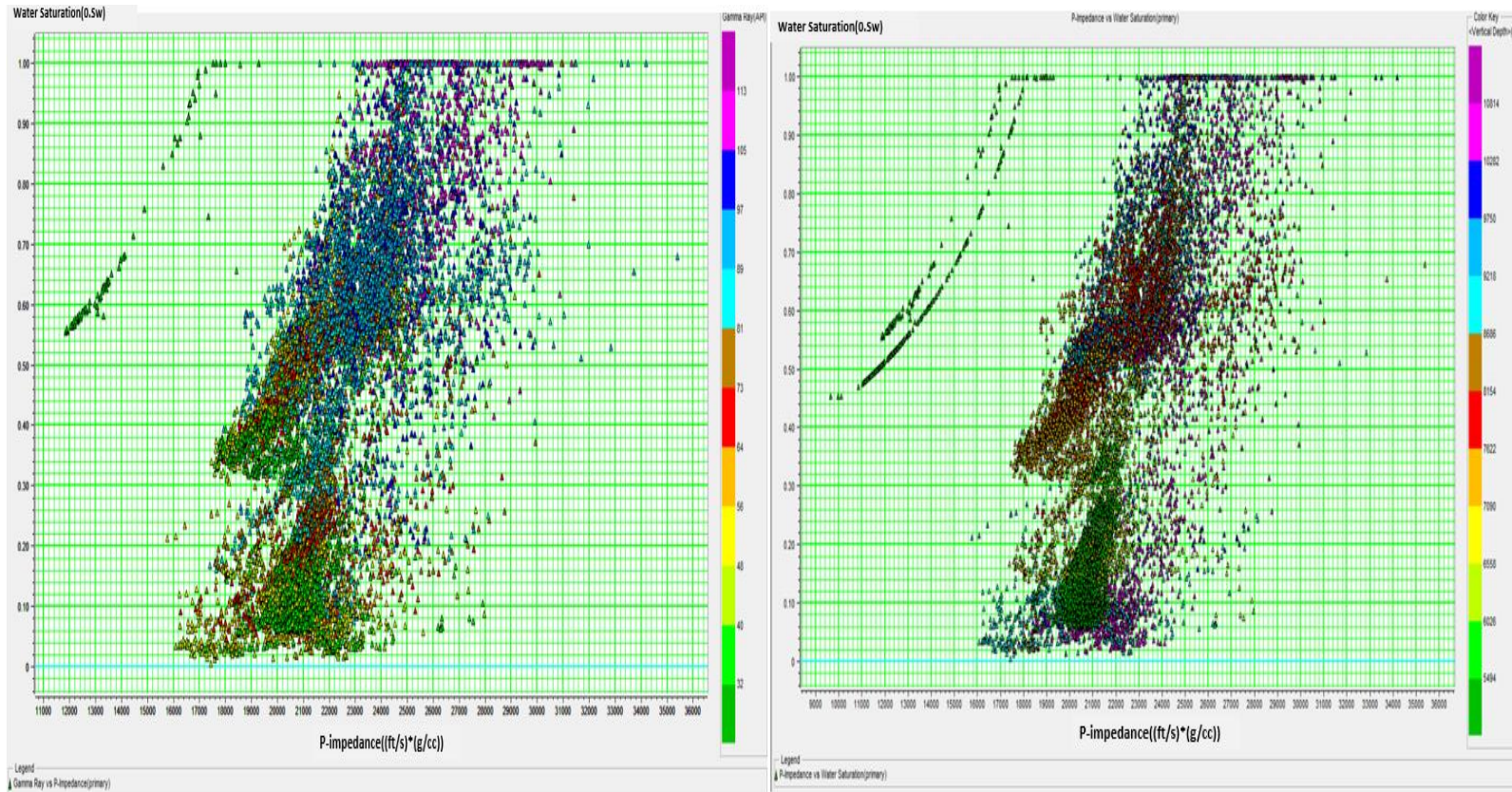


Figure 10: Crossplot of Water Saturation versus Acoustic Impedance for (a) Well 2 (b) Well 12

Table 2: Classification of Acoustic Impedance Range for Inverted Section

Acoustic Impedance Values (Ft/s*g/cc)	Category	Color Code
17021-20191	Very Low	Green
20191-22727	Low	Yellow
22727-25263	Medium	Red
25263-27799	High	Aqua-Marine
27799-30335	Very High	Blue
Above 30335	V.V High	Purple

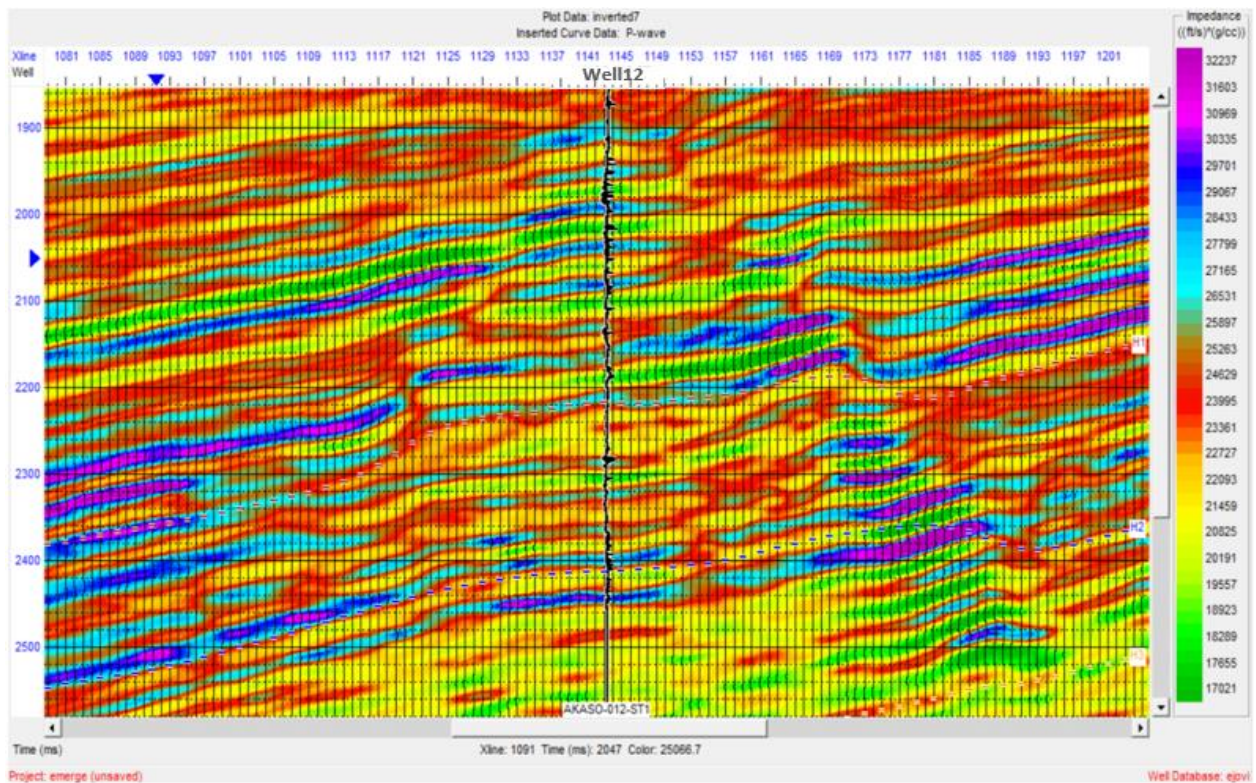


Figure 11: Acoustic Impedance Section at Inline 6925

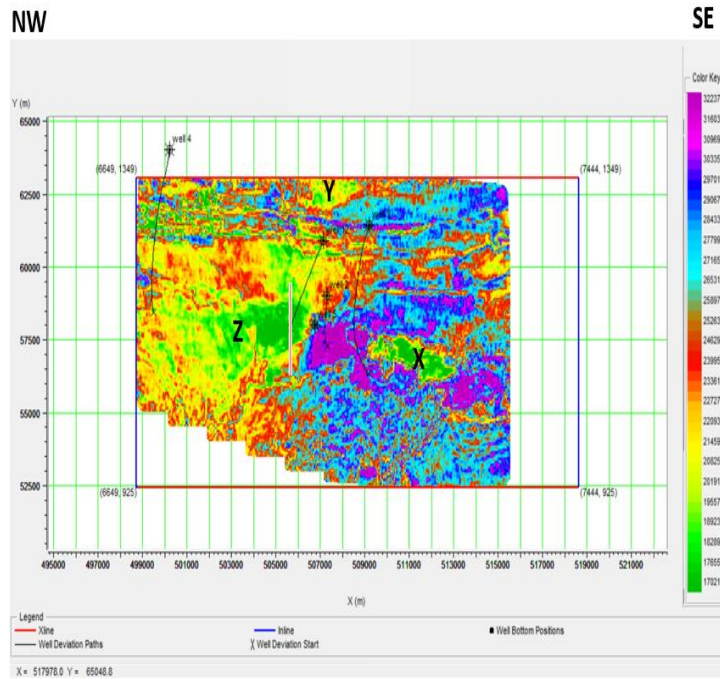


Figure 12: Average Acoustic Impedance Map for Horizon H1

Table 3: Summary of Acoustic Impedance Values in Horizon H1

Impedance range (ft/s*g/cc)	Wells	Porosity (%)	Pore Fluids	Prospect
17201-22000	Well4 Well5 Well12	0.17 0.19 0.34	Oil Oil Oil	X, Y and Z
22500-24500	No well	-----	-----	-----
23500-31608	Well2 Well3	0.22 0.17	Oil Oil	-----

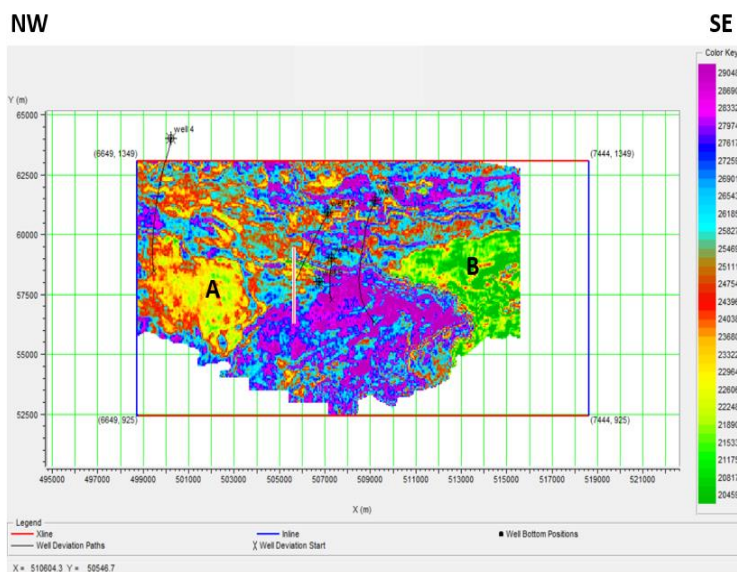


Figure 13: Average Acoustic Impedance Map for Horizon H2

Table 4: Summary of Acoustic Impedance Values in Horizon H2

Impedance Range (ft/s*g/cc)	Wells	Porosity (%)	Pore Fluids	Prospect
20876-22500	Well4 Well12	0.18 0.27	Oil Oil	A and B
22500-24500	No well	-----	-----	-----
23500-29623	Well2 Well3	0.21 0.17	Oil Oil	-----

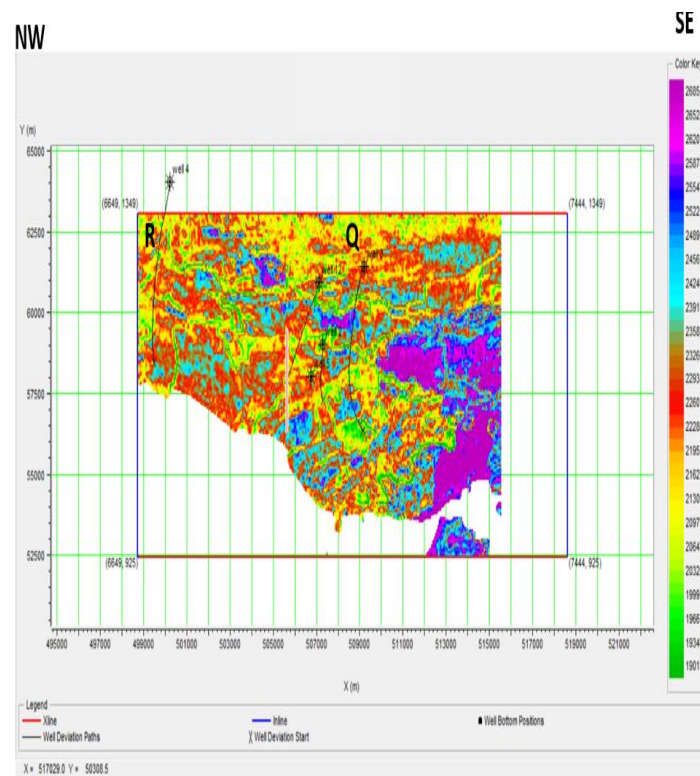


Figure 14: Average Acoustic Impedance Map for Horizon H3

Table 5: Summary of Acoustic Impedance value in Horizon H3

Impedance Range (ft/s*g/cc)	Wells	Porosity (%)	Pore Fluids	Prospect
19013-22280	Well2 Well3 Well12	0.19 0.26 0.12	Oil Oil Oil	Q and R
22280-23587	Well4	0.20	Oil	-----
23587-26854	No well	-----	-----	-----

Correlating depth map and acoustic impedance map (Figure 15) prospect Z falls within the structural high as shown in the depth map for horizon H1 and prospect Q falls on an anticlinal structure as shown in the depth map for horizon H3 (Figure 16).

1.4 Conclusion

Model based seismic inversion has been successfully carried out with the aid of crossplot analysis to characterize the area of study. Acoustic impedance values of 24500-27500(ft/s)*(g/cc), represents shale layers and 17500-24000(ft/s)*(g/cc), represent sand layer (depending on the saturating fluids). Porosity increases as acoustic impedance decreases and water saturation increases as acoustic impedance increases.

The acoustic impedance maps generated shows area of low acoustic impedance (green to yellow color) corresponding to pay sands while area of high acoustic impedance (red, purple and blue color) as shale based on the crossplot. The Areas of low acoustic impedance are classified as hydrocarbon bearing zones having high porosity as established from the Crossplot analysis.

Six prospects A, B, Q, R, X, Y and Z were mapped on the average impedance maps. Comparing the acoustic impedance map and the depth map generated, prospect Q correspond to areas where there is fault assisted closure, and prospect Z correspond to area of structural high. Most of the wells used for the inversion falls within the region of low acoustic impedance area which validates the results of the inversion.

1.5 Recommendation

From the study it was observed that the areas of structural high in the southeastern part and fault assisted anticlinal structure in north central part corresponds to area of low acoustic impedance from the maps generated. These areas are located at the following coordinates and depths; (508000, 62000) 2545.08m, and (506000, 58000) 2773.68m. These areas are suspected to harbor hydrocarbon and it is therefore necessary to carry out further geologic and geophysical interpretations to further confirm these prospects.

Acknowledgement

This research work was carried out under the supervision of Dr. J.O. Amigun of the Department of Applied Geophysics, Federal University of Technology Akure, who made sure I brought out the best from this work. My thanks goes to Mr Uche for his assistance during the course of this project.

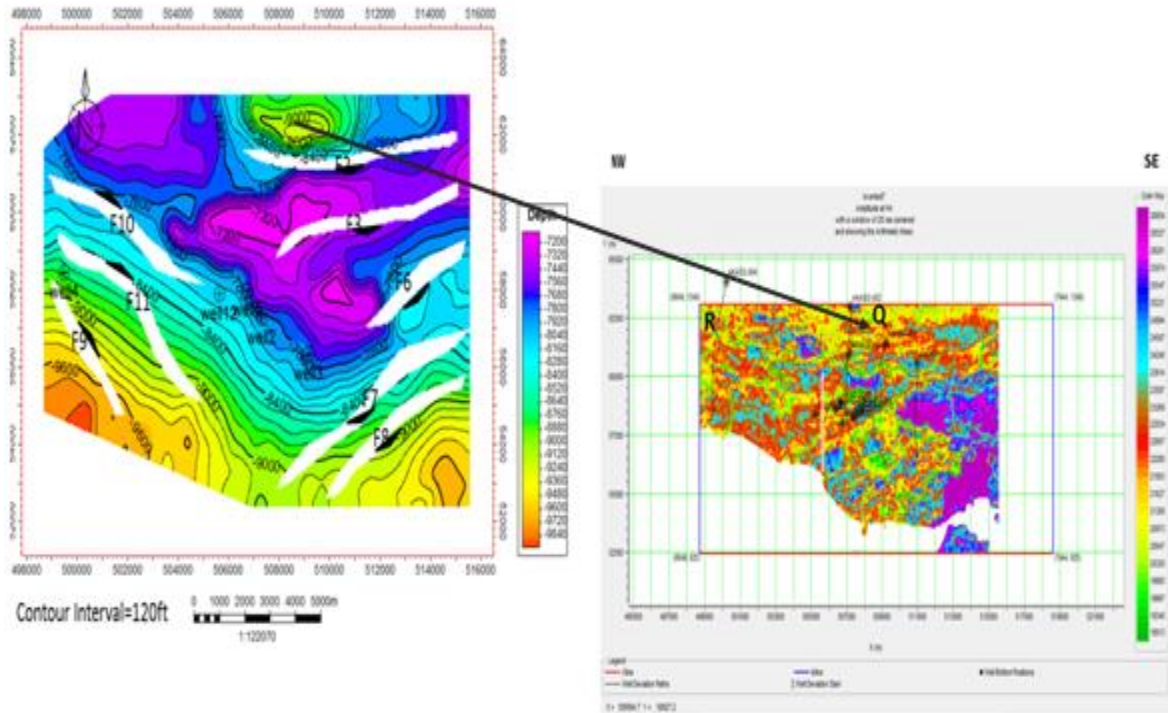


Figure 15: Correlation between the Depth Map and Acoustic Impedance Map of Horizon

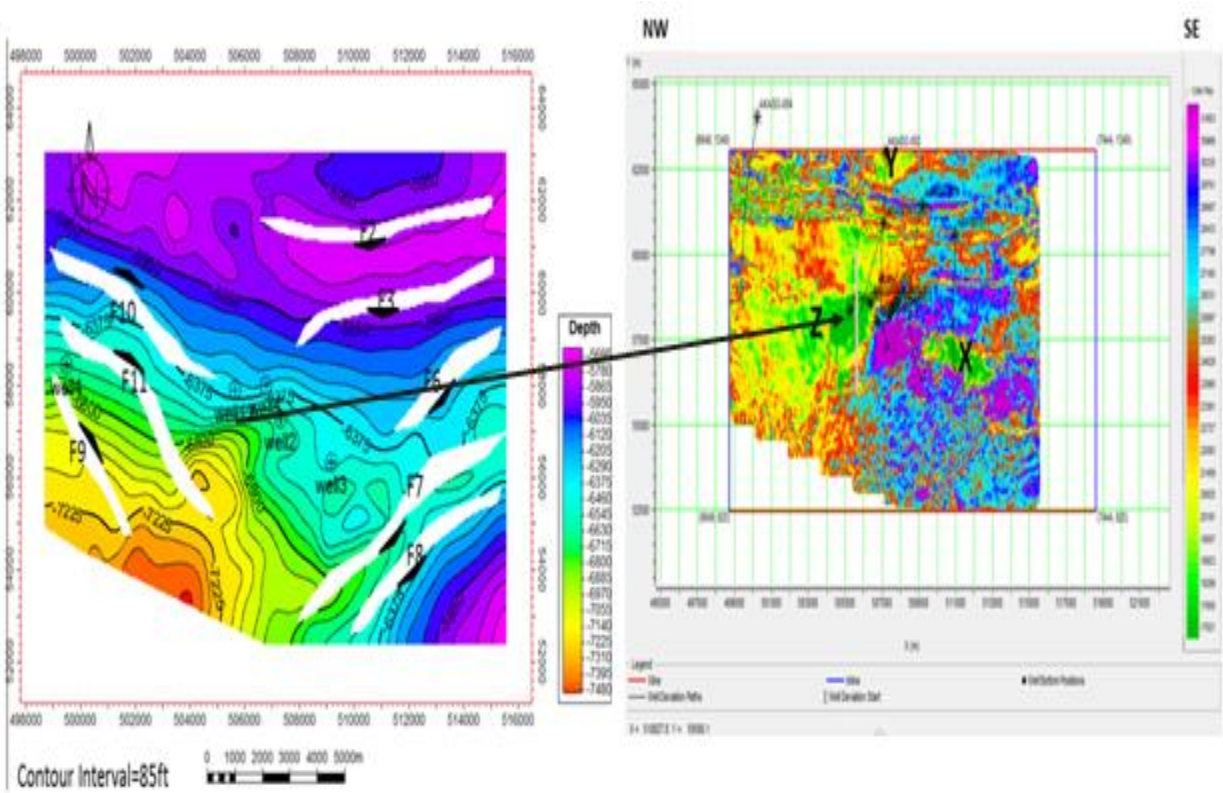


Figure 16: Correlation between the Depth Map and Acoustic Impedance Map of Horizon H1

References

- [1]. Avadhani, V.L., Anandan, M., Thattacherry, B.J., Murthy, K.S., Gariya, B.C., and Dwivedi A.K., (2006). Acoustic impedence as a lithological and hydrocarbon indicator: The Leading Edge. Vol.25, No.07, p.854-858.
- [2]. Badri, M., Svendsen, M., and Egan, M., (2002). Reducing drilling risk through improved seismic imaging. Utilizing new signal-sensor acquisition technology: AAPG Annual International Meeting, Cairo, Egypt.
- [3]. Doust, H., and Omatsola, E.M., (1990). Niger Delta, in, Edwards, J. D., and Santogrossi, P.A., eds., Divergent/passive Margin Basins, AAPG Memoir 48: Tulsa, American association of Petroleum geologist, p.239-248.
- [4]. Evamy, B.D., Hareboure, J., Kamerling, P., Knaap, W.A., Molloy, F.A., and Rowlands, P.H., (1978). Hydrocarbon habitat of Tertiary Niger Delta: American Association of Petroleum Geologist Bulletin, Vol 682, p.277-298.
- [5]. Hampson and Russell Software Services Ltd., (1999). STRATA.
- [6]. Mitchele, L.W., Turtle, R., Charpentier., and Michael, E.B., (1999). The Niger Delta petroleum system: Niger Delta Province, Nigeria, Cameroon and Equatorial Guinea, Africa. USGS. Denver Colorado, Open/file report 99-50-H.
- [7]. Murat, K., (1972). Stratigraphy and paleogeology of crateous and lower tertiary in Southern Nigeria: Proceeding first conference on African Geology, Ibadan 1970, proceeding, Hs: Ibadan University press, p.251-266.
- [8]. Short, K.C and Stauble, J., (1967). Outline geology of the Niger Delta: American Association of Petroleum Geologist Bulletin, vol.5, p.761-779.
- [9]. Shrestha, R. K., and Boeckmann, M. K. (2002, October). Stochastic seismic inversion freservoir modeling. In 2002 SEG Annual Meeting, p.2
- [10]. Singh, H., Subbrayudu, K., Mohorana, A., Singh, M.K., and Kumar, A., (2013). A deterministic approach to reservoir characterization through quantitative interpretation: A case study from hearra field, western offshore India: Society of petroleum geophysics 10th biennial international conference and exposition, p.427.
- [11]. Stacher, P., (1995). Present understanding of the Niger Delta hydrocarbon habitat, in Oti, M.N., and Postma, G., eds Geology of Deltas: Rotterdam, A.A. Balkema, p.257-267.